ELSEVIER

Contents lists available at ScienceDirect

# Electrochimica Acta

journal homepage: www.elsevier.com/locate/electacta



# Synthesis and performance of nanostructured silicon/graphite composites with a thin carbon shell and engineered voids



Maziar Ashuri <sup>a, b</sup>, Qianran He <sup>a, b</sup>, Yuzi Liu <sup>c</sup>, Satyanarayana Emani <sup>a, b</sup>, Leon L. Shaw <sup>a, b, \*</sup>

- <sup>a</sup> Department of Mechanical, Materials and Aerospace Engineering, Illinois Institute of Technology, Chicago, IL 60616, USA
- <sup>b</sup> Wanger Institute for Sustainable Energy Research (WISER), Illinois Institute of Technology, Chicago, IL 60616, USA
- <sup>c</sup> Center for Nanoscale Materials, Argonne National Laboratory, Lemont, IL 60439, USA

#### ARTICLE INFO

Article history:
Received 28 August 2017
Received in revised form
29 September 2017
Accepted 30 October 2017
Available online 16 November 2017

Keywords: Lithium-ion battery Anode Silicon High-energy ball mill

#### ABSTRACT

Utilizing silicon as an anode material for Li-ion batteries has been the subject of many studies. However, due to the huge volume change of silicon during lithiation, the electrochemical performance of silicon is poor. Here, we have investigated a novel yet simple approach to synthesize nanostructured silicon/graphite composites with a carbon coating and engineered voids. High-energy ball mill is employed to convert micrometer-sized silicon and graphite to nanostructured silicon/graphite composite building blocks, while a thin carbon coating is applied to encapsulate these composite agglomerates, followed by partial etching of silicon to create engineered voids inside the composite agglomerates. The batteries made with this tailored nanostructure exhibit improved electrochemical performance over the counterparts made with silicon nanoparticles and exhibited a specific capacity of ~1800 mA h  $\rm g^{-1}$  discharge capacity at the first cycle, 580 mA h  $\rm g^{-1}$  after 40 cycles, and 350 mA h  $\rm g^{-1}$  after 300 cycles. This study has established a novel method scalable at industry environment and capable of producing low cost Si anodes and clearly shown that the cycle stability of the tailored nanostructure improves with increasing engineered voids in the range we have investigated.

© 2017 Elsevier Ltd. All rights reserved.

#### 1. Introduction

Silicon is one of the most prominent materials for lithium-ion batteries [1,2] and has been subject of broad studies since two decades ago [3,4]. However, the problem of volume expansion during lithiation causes the huge expansion in the structure and finally resulted in peeling off and poor cycling stability [1]. Many efforts have been made to solve this problem. These strategies include core-shell structures [5–7], yolk-shell designs [8], hollow spheres with or without conductive coating [9,10], and making composites with other conductive materials [11,12]. However, most of these proposed methods require expensive equipment or precursor and need multiple steps of synthesis, which make them not suitable for scaling up for industrial applications. Among the aforementioned solutions, preparing composites of silicon with other conductive materials appears to be feasible and reasonable. In this regard, carbon-coated silicon and silicon/graphite (Si/Gr)

composites have been studied extensively by Yoshio's research group in Japan [13-21]. Si/graphene and Si/nanographite sheet composites have also been studied extensively [22-26], because graphene have outstanding electronic conductivity and can also serve as a substrate to constrain volume expansion of Si particles during cycles. In addition, carbon nanotubes (CNTs), carbon nanofibers (CNFs) and fine graphite particles can all provide electron transport pathways and serve as effective substrates to constrain volume expansion of Si particles during cycles [27-29]. These different carbon-containing composites have significantly improved the electrochemical performance of Si anodes. For example, Zhang, et al. [27], have developed a synthesis procedure to produce a low-cost Si/CNT&CNF composite made of carboncoated Si nanoparticles interweaved with CNTs and CNFs, denoted as Si@C/CNTs&CNFs. The obtained composite displays high capacities with superior cycling stability (1195 mA h  $\mathrm{g}^{-1}$  after 50 cycles at 300 mA  $g^{-1}$ ) [27].

Silicon-based composites mixed with non-carbon materials have also been investigated extensively. These composites include Si/ceramic, Si/polymer, Si/metal, and Si/intermetallic composites. This group can offer positive surprises if the design principles to

<sup>\*</sup> Corresponding author. Department of Mechanical, Materials and Aerospace Engineering, Illinois Institute of Technology, Chicago, IL 60616, USA. E-mail address: lshaw2@iit.edu (L.L. Shaw).

solve the Si anode problems are followed [30–34]. An interesting example of Si/ceramic/metal/carbon composites is the a-Si-SiO<sub>x</sub>/Cr/ C composite made lately by Li et al. [30]. A simple, scalable two-step method is used to synthesize such a composite. The commercial SiO powder is first subjected to disproportionation reaction at 1000 °C for 3 h to form the Si/SiO<sub>x</sub> nanoscale mixture which is then ball milled with micro-sized Cr and graphite powders. The obtained composite exhibits a high specific capacity (810 mA h  $g^{-1}$ ) with capacity retention close to 100% over 200 cycles at a current density of 100 mA  $g^{-1}$ . For comparison, other composites without graphite (a-Si-SiO<sub>x</sub>/Cr), without Cr (m-c-Si-SiO<sub>x</sub>/graphite), and without Cr and graphite (m-c-Si-SiO<sub>x</sub>) have also been synthesized and tested. All of them have displayed poor cycling stability. It is found that the high hardness of Cr powder has led to the formation of a-Si-SiO<sub>x</sub> in very fine particle sizes during ball milling. As a result, small volume change takes place per particle during cycles, thereby minimizing the loss of particle contact and the stress causing the fracture and re-formation of SEI layers [30].

Here, we have investigated a novel and simple approach to synthesize silicon/graphite nanocomposites with a carbon shell, followed by etching the composites with sodium hydroxide (NaOH) solution to create engineered voids for accommodating the huge silicon expansion during lithiation. The final product (designated as Si/Gr@void@C) exhibits better performance comparing to silicon nanoparticles as well as the previous reports on Si/Gr composites which do not employ etching. The improved performance is attributed to the engineered voids formed in the structure which act as cushion for the huge volume change of silicon (about 400% of its original value) during lithiation. The 300 charge/discharge cycles achieved with Si/Gr@void@C is among the longest ones for Si anode studies published to date. Furthermore, our proposed method is scalable at industry environment because our work only needs lowcost micrometer-sized Si powder with simple experimental procedure. In addition, this study demonstrates unambiguously that the cycle stability of Si/Gr@void@C composites depends strongly on the engineered voids in their structure. As the volume of the engineered void increases in the range we have studied, the cycle stability improves.

#### 2. Experimental details

## 2.1. Synthesis of Si/Gr@void@C composites

Micrometer-sized silicon powder (99.9995% trace metals basis, Sigma Aldrich) and graphite powder (BNB90 (AA-130), TIMCAL) were mixed together with a weight ratio of 9:1. After complete mixing of silicon and graphite in a vial, the mixed powder was loaded in a stainless steel canister inside a glove box filled with Ar. Stainless steel balls were utilized as milling medium and the charge ratio (ball-to-powder weight ratio) was 20:1. The loaded canister was transferred to a SPEX® 8000M Mixer/Mill® machine and the mixed powder was milled for 6 h. To avoid overheating and thus prevent caking, milling was stopped for 10 min after each 1-h milling. After high-energy ball milling the canister was transferred to the Ar-filled glove box again for unloading. The collected powder was used for carbon coating.

The carbon coating was achieved using pyrrole as the precursor. The coating procedure entailed mixing 0.5 g of the ball milled powder with 1 mL pyrrole inside a quartz crucible. The mixture was stirred with a spatula to obtain uniformity before the crucible was covered with a copper foil. The crucible was then loaded into a stainless steel autoclave which was completely sealed in the glove box under the Ar atmosphere. After this step, the autoclave was transferred to a furnace and heated to 550 °C for 5 h to form the carbon-coated silicon/graphite composite (designated as Si/Gr@C).

The heating and cooling rates were chosen as 5 °C per min.

The Si/Gr@C nanocomposite formed through pyrrole coating was etched with a 0.5 M sodium hydroxide (NaOH) solution. Different etching conditions (e.g. different times and temperatures) were evaluated in order to find a suitable etching condition to generate engineered voids. After etching, powder was washed with deionized water and dried at 80 °C for 12 h. The resulting powder was denoted as Si/Gr@void@C for the following electrochemical evaluation. Fig. 1 summarizes the synthesis steps.

#### 2.2. Electrochemical measurements

Si/Gr@void@C nanocomposites were employed as the active material and mixed with carbon black (CB, TIMCAL) and polyacrylic acid (PAA, average molecular weight 1800, Sigma Aldrich) in a weight ratio of 60:20:20, respectively. The mixture was grinded using an agate mortar and pestle and then N-methyl-2-pyrrolidone (NMP) was added to form a uniform slurry which was subsequently applied to a copper foil. The painted foil was vacuum-dried in an oven at 120 °C for 12 h. After drying, the foil was punched to make working electrodes for fabrication of 2032 coin cells. The loading of the active material in the electrode was about  $0.7 \text{ mg cm}^{-2}$ . Lithium metal chips were used as the counter and reference electrode. while the electrolyte was 1 M LiPF<sub>6</sub> salt in ethylene carbonate (EC)diethylene carbonate (DEC) with 1:1 vol ratio and 10 vol % fluoroethylene carbonate (FEC) as the additive. Celgard 2325 membrane was used as the separator. Batteries were discharged/charged with the Neware® battery test system between 0.005 and 1.5 V vs. Li/Li<sup>+</sup> at different current densities. Current densities were calculated based on the weight of the active material (Si/Gr@void@C) in the electrode, while specific capacities were determined either based on the weight of the active material or based on the weight of Si in the electrode. The use of different weight bases for evaluating specific capacities is to facilitate discussion and comparison and will be indicated clearly in all the relevant figures. Cyclic voltammetry (CV) test was performed with Parstat 4000 (Princeton Applied Research) from 0.005 to 1.5 V vs. Li/Li<sup>+</sup> at a scan rate of  $0.05 \text{ mV s}^{-1}$ .

For the comparison purpose and to obtain a better understanding of the properties of Si/Gr@void@C, an additional set of half cells with the working electrode made of Si nanoparticles (>99%, 70—130 nm) from NanoAmor® were fabricated. Li metal chips were used as the counter and reference electrode in these half cells and the entire process of coin cell fabrication (such as the ratios of the active material to binder and carbon black, type of the separator and electrolyte, etc.) was identical to that of Si/G@void@C half cells.

#### 2.3. Material characterization

JEOL JSM-5900LV (JEOL Ltd., Tokyo, Japan) scanning electron microscope (SEM) with accelerating voltage of 20 kV was used to investigate the powder particle size and morphology. Samples were first coated with gold using a sputter coater before SEM examination to avoid charging. JEOL JEM-3010 transmission electron microscope (TEM) was employed to further determine the microstructure of the powder particles. Furthermore, the elemental distribution of Si/Gr@void@C was studied using an energy-filtered TEM (EFTEM) in the Center for Nanoscale Materials (CNM) at Argonne National Laboratory (ANL). A Gatan environmental transfer holder was employed to keep the TEM specimen from air and moisture before loading the specimen into EFTEM for the elemental distribution analysis. X-ray diffraction (XRD) patterns were collected with Bruker D2 Phaser with Bragg-Brentano geometry in the  $2\Theta$  range of  $25^\circ$  to  $100^\circ$  with Cu  $K\alpha$  radiation (1.54056 Å). Raman spectra was collected using Renishaw inVia

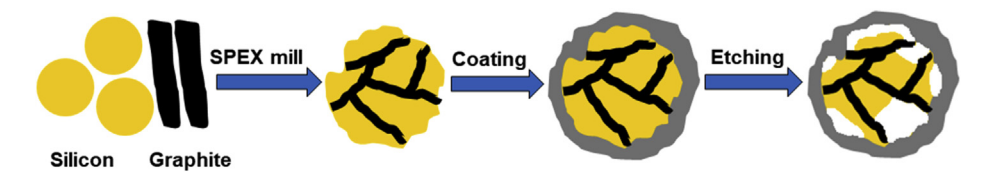


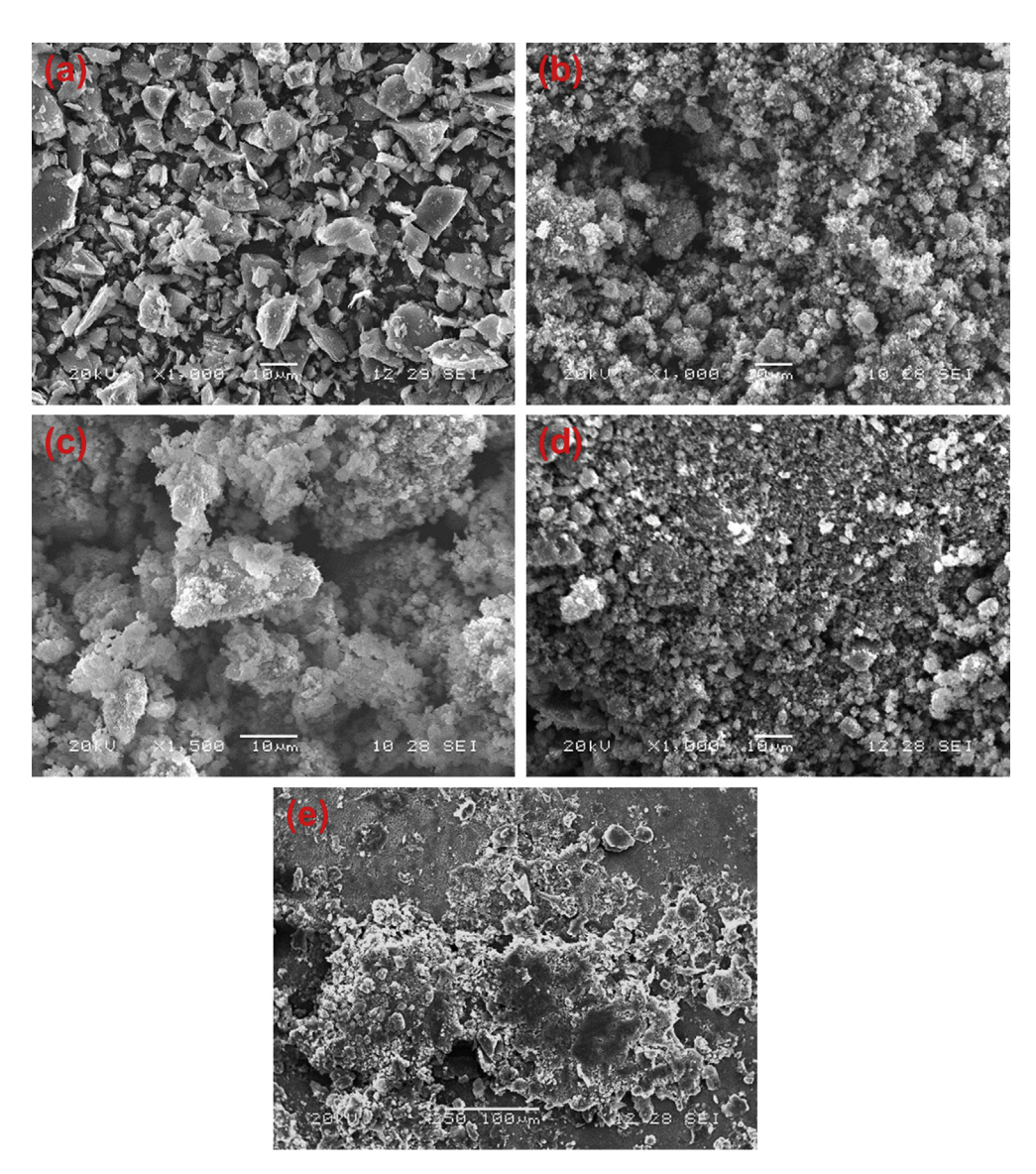
Fig. 1. Schematic of Si/Gr@void@C composite synthesis procedure.

confocal Raman microscope equipped with a CCD detector. The excitation wavelength was 514 nm with the grating of 1800 lines per mm. The data was collected and processed with Wire 3.4 software. Thermogravimetric analysis (TGA) was also conducted to ensure that there is no oxidation of graphite during high-energy ball milling. The TGA machine is Mettler-Toledo TGA-SDTA851e and the TGA experiments were conducted under a flowing dry air with a 5 °C per min heating rate. Brunauer, Emmett and Teller (BET) measurement was performed to determine the specific surface area (SSA) of Si samples at different processing stages with a two-channel Nova Quantachrome 2200e surface area & pore size

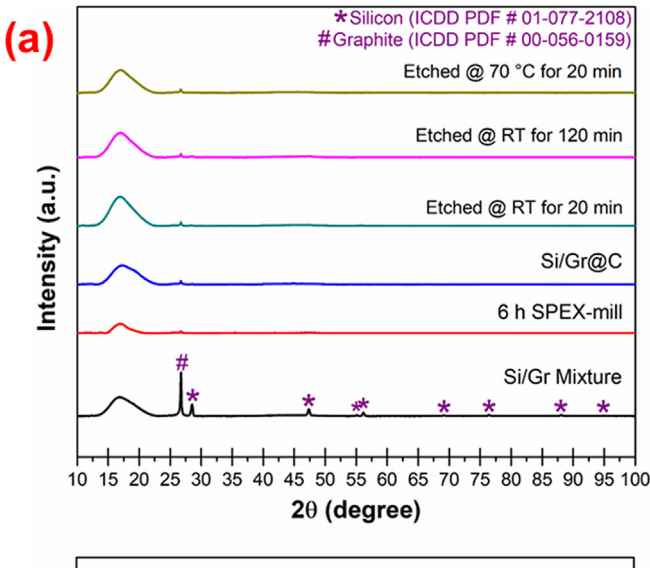
analyzer.

#### 3. Results and discussions

In Fig. 2 we can track the powder morphology in different stages of synthesis. Fig. 2(a) illustrates the SEM image of silicon and graphite mixtures before ball milling. Both Si and graphite particles are micrometer sized with irregular shape. Most of the particles have sizes in the range from 1  $\mu$ m to 15  $\mu$ m. Fig. 2(b) shows the SEM image of Si/Gr powder after 6 h milling. The powder is significantly agglomerated after ball milling, but without forming a cake. The



**Fig. 2.** SEM images of (a) Si/Gr powder mixture before ball milling, (b) Si/Gr powder after ball milling for 6 h, (c) Si/Gr@C using pyrrole as the precursor, (d) sample *c* etched for 20 min, and (e) sample *c* etched for 2 h. Etching is conducted at room temperature with 0.5 M NaOH solution.



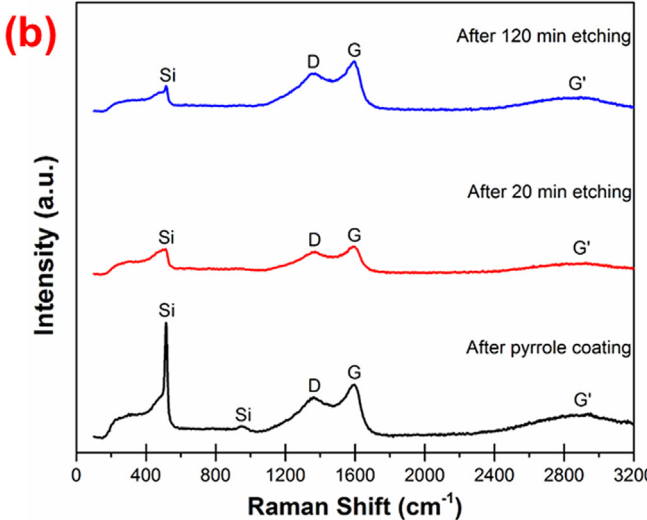


**Fig. 3.** (a) XRD patterns of Si/Gr@void@C composites at different synthesis steps as indicated, including the Si/Gr mixture, ball milled for 6 h, coated with pyrrole as the precursor, etched at room temperature for 20 min and 120 min, and finally etched at 70 °C for 20 min. The board peak at ~16.7° is from the capillary tube used to prevent the oxidation of powders during XRD data collection. (b) Raman spectra of Si/Gr@void@C composites at different synthesis steps (coated with pyrrole as the precursor, etched at room temperature for 20 min and 120 min).

sizes of agglomerates vary widely ranging from as small as 1  $\mu$ m to as large as 30  $\mu$ m. However, the primary particles that constitute agglomerates are less than 1  $\mu$ m and many of them are in the range from 200 to 400 nm. The substantial reduction in the primary particle size induced by high-energy ball milling is consistent with the primary function of high-energy ball milling, i.e., repeated deformation, fracture and cold welding of brittle materials [35,36].

The SEM image of Si/Gr composites coated with C using pyrrole as the precursor is shown in Fig. 2(c). The morphology of the coated powder is similar to that of the ball milled powder, suggesting that the carbon coating, if present, is very thin. This is consistent with our prior study on carbon coating of hollow Si nanospheres using pyrrole as the precursor [6]. In that prior study, it is shown that the carbon coating derived from pyrrole is about 5–20 nm thick [6,37]. Fig. 2(d) and (e) are captures from the Si/Gr@void@C samples etched using NaOH at room temperature. The morphology of the powder remains similar to that before etching, indicating that

NaOH etching does not cause any visible change based on the analysis of SEM. Thus, other analytical methods, such as TEM, XRD and Raman, should be utilized to provide supplemental information about the changes in powder characteristics after each synthesis step.

Fig. 3(a) displays XRD patterns after each synthesis step. At the as-mixed condition, silicon peaks can be easily detected, matching crystalline silicon (ICDD PDF card 01-077-2108) very well. However, only one major peak at ~27° is detected for graphite. This is due to the low concentration of graphite in the mixture. All of the Si peaks, however, disappear after 6 h ball milling, suggesting that crystalline Si has been converted to amorphous. The intensity of graphite peak at ~27° is also reduced drastically, suggesting that most of graphite has become amorphous too. This is consistent with a previous study [35], showing that graphite approaches the amorphous state after 6 h ball milling. In another previous study [36], we have demonstrated that long milling time (e.g., 24 h) could result in formation of crystalline SiC in situ during high-energy ball milling of Si and C mixture at room temperature. However, if the high energy ball milling time is short (<24 h), no SiC formation is observed [36]. The present study is consistent with the prior investigation, i.e., there is no sign of the formation of crystalline SiC, confirming that the 6 h ball milling time is not long enough to induce in-situ formation of crystalline SiC during ball milling. Coating with pyrrole did not change the amorphous structure of the powder, indicating that carbonization temperature of pyrrole at 550 °C is not high enough to crystallize amorphous Si and the carbon coating derived from pyrrole is amorphous in nature as well. The latter is consistent with our previous studies [6,37]. After etching with NaOH solution, the composites remain to be amorphous.

Fig. 3(b) exhibit the Raman spectra of Si/Gr@C composites before and after etching. The presence of Si bands is observed in all conditions, confirming that Si is present as an amorphous phase after ball milling since no XRD peaks of Si are observed after 6 h ball milling (Fig. 3(a)). In addition to silicon bands, D, G and G' bands are seen. D band is due to the presence of disordered carbon, while G band represents the graphitized carbon [38]. The formation of these bands suggest the formation of carbon coating derived from pyrrole, consistent with our previous study on carbon-coated hollow silicon nanospheres [6]. After the etching the intensities of these bands become sharper, while silicon bands become weaker. The reason is the removal of some silicon during NaOH etching.

Two other important questions regarding the effects of highenergy ball milling are: (i) is graphite oxidized during ball milling? and (ii) is graphite mixed well with Si? To answer the first question, we have conducted TGA analysis of Si, graphite and their composites with different processing conditions. First, pure graphite powder was high-energy ball milled for 2 h and 6 h, and then subjected to TGA analysis under a flowing dry air atmosphere. Second, pure Si powder was also high-energy ball milled for 2 h and 6 h, and then subjected to the same TGA analysis as the pure graphite. Finally, Si/Gr mixture (9:1 wt ratio) was high-energy ball milled for 2 h and 6 h, and then subjected to the same TGA analysis as the pure graphite and Si. The TGA curves of these different samples are summarized in Fig. 4. Several interesting trends are noted from Fig. 4. The reactivities of both pure graphite and Si increase with increasing the ball milling time, as evidenced by the reduction of both the onset and completion temperatures for graphite oxidation (Fig. 4(a)) and the increase in weight gain for pure Si as the ball milling time increases (Fig. 4(b)). Fig. 4(a) also proves that there is little or no oxidation of graphite during highenergy ball milling. Otherwise, there will be no graphite for analysis. Finally, Si/Gr composites display very intriguing results. For the Si/Gr composite ball milled for 2 h, it shows slight weight gain

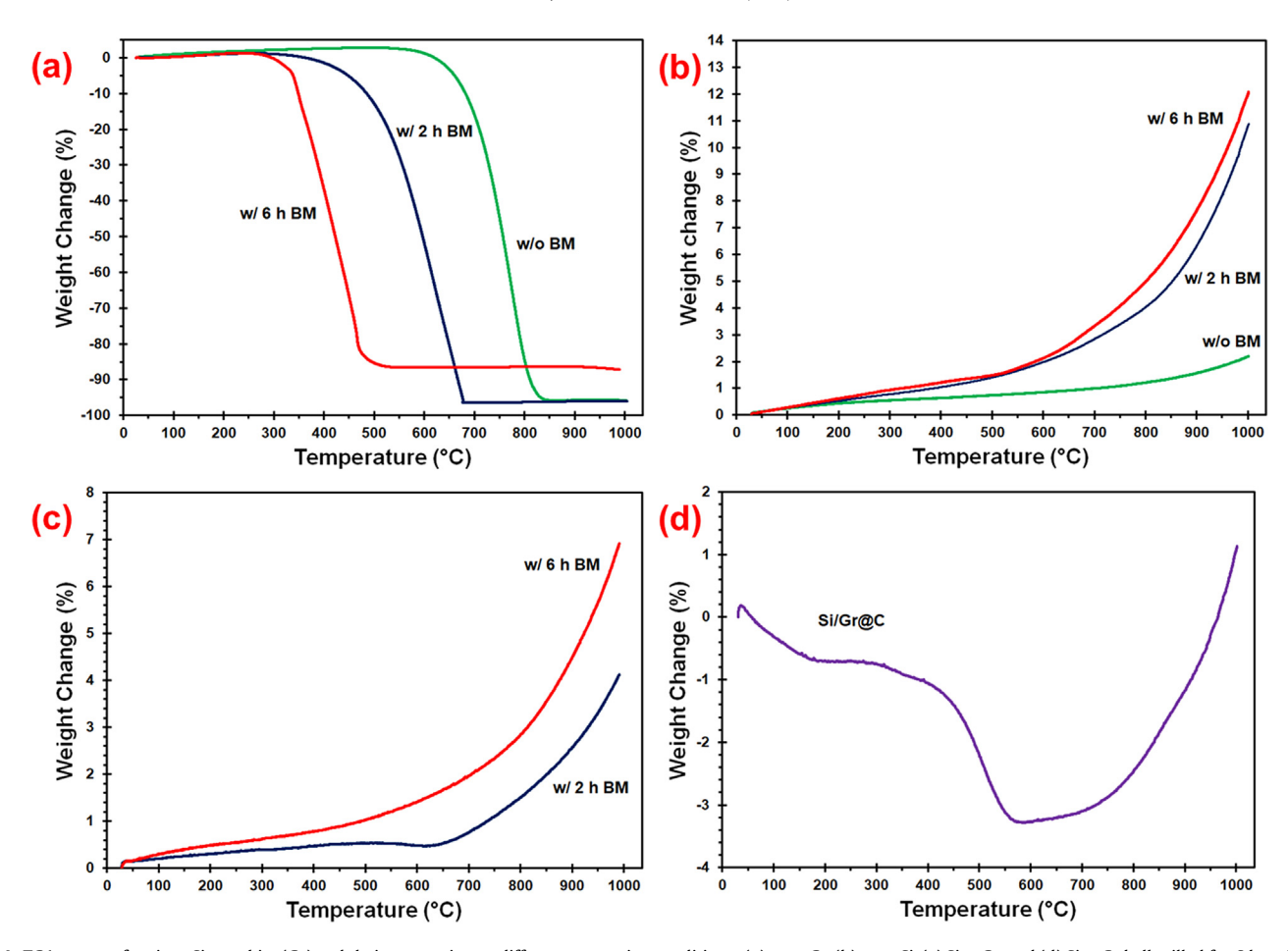


Fig. 4. TGA curves of various Si, graphite (Gr) and their composites at different processing conditions: (a) pure Gr, (b) pure Gr, (c) Gr, and (d) Gr and their content with carbon using pyrrole as the precursor. BM stands for high-energy ball milling.

**Table 1** EDS results of Si/Gr after 6 h ball milling.

Spectrum ID	С	Si	Fe	Total
Spectrum 1	27.69	71.39	0.92	100.00
Spectrum 2	22.27	77.73	0.00	100.00
Spectrum 3	0.00	100.00	0.00	100.00
Spectrum 4	25.59	74.41	0.00	100.00

first, then slight weight loss at about 580-630 °C, and finally weight gain again (Fig. 4(c)). The weight loss at the intermediate temperature range is clearly due to the presence of graphite because Si will not have any weight loss as shown in Fig. 4(b). Furthermore, the total weight gain of Si/Gr is smaller (4.1% for 2 h ball milling and 6.9% for 6 h ball milling) than pure Si (10.9% for 2 h ball milling and 12.1% for 6 h ball milling), again due to the presence of graphite and its oxidation. However, a simple linear addition of the TGA data of 90% Si with the TGA data of 10% graphite does not match the TGA data of the Si/Gr composite, indicating that some graphite has been embedded inside Si agglomerates and does not get oxidized or get oxidized at higher temperatures due to the protection of the Si matrix. Embedding part of the graphite inside Si agglomerates is consistent with the nature of high-energy ball milling – repeated deformation, fracture and cold welding [35,36]. After carbon coating using pyrrole as the precursor the TGA curve (Fig. 4(d)) exhibits significant change from the Si/Gr composite ball milled for 6 h (Fig. 4(c)). Weight loss becomes dominant from room temperature to about 580 °C because the carbon coating is exposed to oxygen directly. Based on the weight loss data, it is estimated that the pyrrole coating process has introduced about 4 wt % carbon to the Si/Gr composite (see Supplementary Materials for details).

To answer whether graphite is mixed well with Si after highenergy ball milling, we use SEM/EDS to assess the average compositions at different locations of the sample. Fig. S1 in Supplementary Materials shows a SEM image of a Si/Gr composite after 6 h ball milling and the locations from which the EDS data are collected are indicated. The EDS data obtained from these locations are summarized in Table 1. Note that the Si/Gr composite powder was dispersed on a conductive carbon tape when the EDS data was collected. As a result, some carbon signals could come from the carbon tape if the powder layer was very thin. Therefore, the data in Table 1 can only be used to deduce the trends of the composition. With this in mind, one can conclude that the average compositions at the locations of Spectra 1 and 2 are close to the average composition of the area indicated by the rectangular box of Spectrum 4, suggesting that at these individual locations graphite and Si are mixed uniformly within 1-µm length scale or smaller. This is consistent with the fact that most of the primary particles of graphite and Si have sizes in the range of  $0.2-0.4~\mu m$  as shown in Fig. 2. However, exception is present, such as at the location of Spectrum 3 where no carbon is found. The electron beam size for the spot EDS analysis is 1 µm and thus it can be said that there is no carbon present in the 1-µm range at this location. In spite of this exception, overall graphite and Si are mixed quite well within 1-µm length scale or smaller after 6 h ball milling.

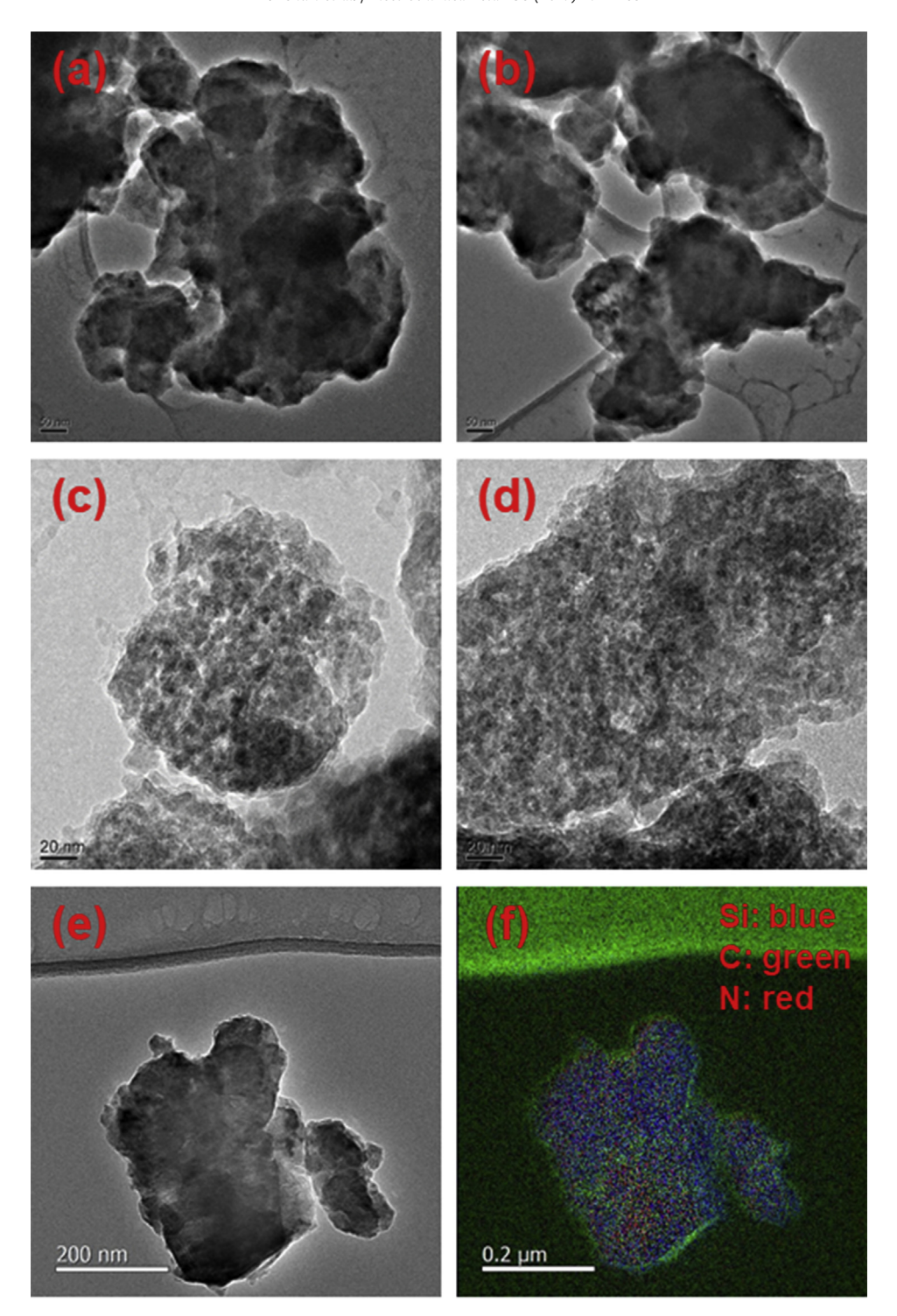
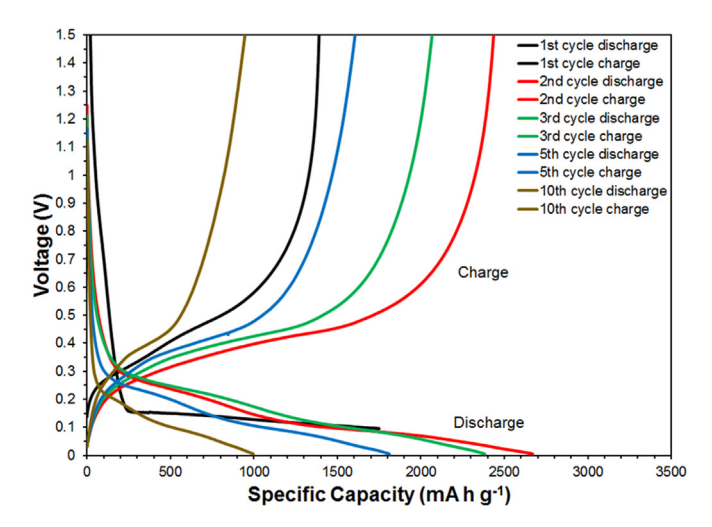


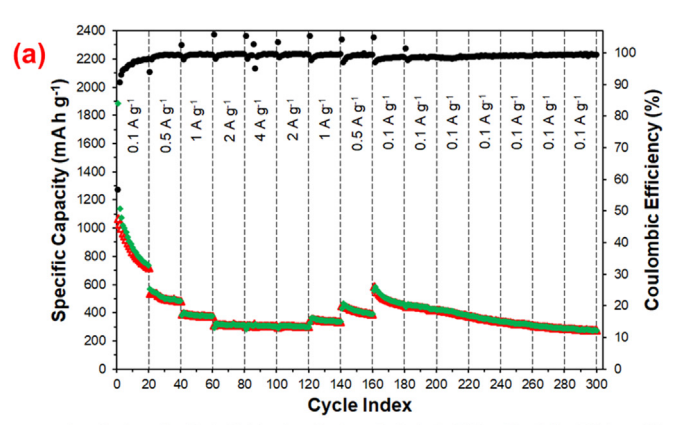
Fig. 5. TEM images of Si/Gr@void@C etched with 0.5 M NaOH solution: (a) at room temperature for 20 min, (b) at room temperature for 2 h, (c) and (d) at 70 °C for 20 min; two images are displayed to show the general trend of different agglomerates, (e) EFTEM image and (f) elemental map of Si/Gr@void@C etched with 0.5 M NaOH solution at room temperature for 20 min. Note that the carbon coating derived from pyrrole contains some nitrogen which enhances the electronic conductivity [37].

**Table 2**Specific surface area (SSA) of various Si powders with different processing conditions.

Sample	Silicon powder	Graphite powder	Si/Gr with 6 h ball milling	Si/Gr@C	Si/Gr@void@C with etching at RT for 20 min	Si/Gr@void@C with etching at 70 °C for 20 min
SSA $(m^2 g^{-1})$	1.2	4.3	7.6	6.6	11.1	269.4



**Fig. 6.** Voltage profile for Si/Gr@void@C etched with 0.5 M NaOH solution at room temperature for 20 min. The current density for charge/discharge cycles was 0.1 A  $\rm g^{-1}$  and the specific capacity was calculated based on the quantity of the active material in the electrode.



 $\Delta \, \mathsf{Specific} \, \, \mathsf{Capacity\text{-}Chg}(\mathsf{mAh/g}) \, \, * \, \mathsf{Specific} \, \, \mathsf{Capacity\text{-}Dchg}(\mathsf{mAh/g}) \, \, \bullet \, \, \mathsf{Chg/DChg} \, \, \mathsf{Efficiency}(\%)$ 

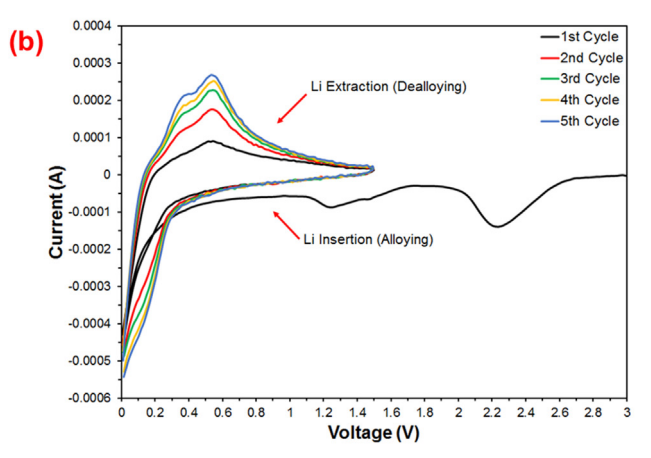


**Fig. 7.** (a) Specific capacity and Coulombic efficiency of Si/Gr@void@C etched with 0.5 M NaOH solution at 70 °C for 20 min at different current densities, and (b) its CV curve at scan rate of 0.05 mV s $^{-1}$ . The specific capacity was calculated based on the quantity of the active material in the electrode.

It should be mentioned that the EDS analysis also reveals the presence of a trace amount of iron in the ball milled sample (below 1 wt %) at some locations (e.g., Spectrum 1). This impurity is introduced to the sample due to the wear of stainless steel balls and

present as debris. However, this impurity has little or no effect on electrochemical performance because most of the powder particles do not have iron debris.

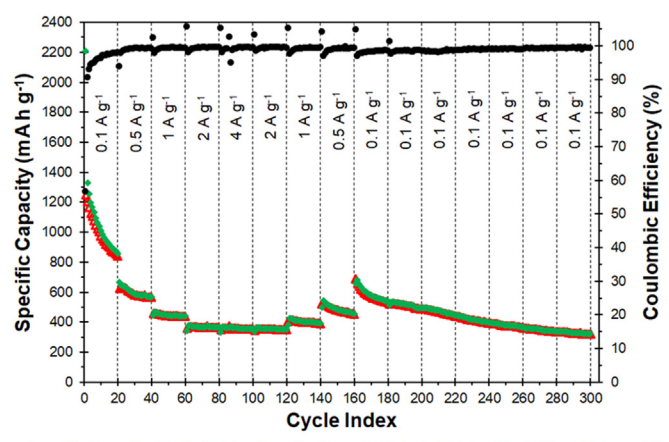
To detect whether there are voids in Si/Gr@void@C, we have employed TEM. Fig. 5(a) and (b) show TEM images of Si/Gr@void@C etched with NaOH at room temperature for 20 min and 2 h, respectively. These images reveal that there are few voids in the sample. The principle of etching Si by a NaOH aqueous solution is described by the following equation [39].

$$Si + 2NaOH + H_2O \rightarrow Na_2SiO_3 + 2H_2\uparrow$$
 (1)

Note that the reaction product of sodium silicate is readily soluble in water and thus can be washed away after etching. Since etching at room temperature leads to few voids inside the composite, we have increased the etching temperature to 70 °C in order to enhance the etching rate. As shown in Fig. 5(c) and (d), increasing the etching temperature to 70 °C has greatly accelerated the etching reaction, leading to obvious presence of many voids within the Si/Gr@void@C composite. Many open channels of about 5 nm in size (represented by bright spots inside agglomerates) are clearly visible for each and every agglomerate. It is worthy of mentioning that the presence of many voids in Si/Gr@void@C is also in good accordance with the fact that many hydrogen bubbles have been observed during etching at 70 °C (see Supplementary Video). To find out the presence of a carbon shell and its thickness at Si/Gr@void@C, elemental mapping using EFTEM has been conducted. As shown in Fig. 5(e) and (f), a carbon shell is present and its thickness is about 10 nm. In addition, Si and graphite are mixed inside the agglomerate, corroborating the proposition that part of graphite is embedded inside the Si matrix after 6 h ball milling based on the observation of the TGA data (Fig. 4).

Supplementary video related to this article can be found at https://doi.org/10.1016/j.electacta.2017.10.198.

BET surface area measurements support the TEM analysis, showing that etching at 70 °C can effectively create voids in Si/Gr@C. As shown in Table 2, the starting Si and graphite micronsized powders have relatively low specific surface area (SSA) with 1.2 and 4.3 m² g⁻¹, respectively. After 6-h ball milling at ambient temperature, the SSA of the Si/Gr powder mixture has increased to 7.6 m² g⁻¹, while carbon coating using pyrrole as the precursor has led to a slight decrease of SSA to 6.6 m² g⁻¹ for Si/Gr@C. Etching using NaOH at room temperature for 20 min has increased SSA to



 $\Delta \, \mathsf{Specific} \,\, \mathsf{Capacity\text{-}Chg}(\mathsf{mAh/g}) \, \bullet \, \mathsf{Specific} \,\, \mathsf{Capacity\text{-}Dchg}(\mathsf{mAh/g}) \, \bullet \, \mathsf{Chg/DChg} \,\, \mathsf{Efficiency}(\%)$ 

**Fig. 8.** The specific capacity and coulombic efficiency of Si/Gr@void@C etched with 0.5 M NaOH solution at 70  $^{\circ}$ C for 20 min. The specific capacity was calculated based on the Si quantity in the electrode.

11.1 m² g⁻¹. However, this increase is very small in comparison with the effect of etching at 70 °C for 20 min, which has increased SSA to 269.4 m² g⁻¹. Clearly, this drastic increase in SSA is due to effective etching of Si particles at 70 °C. Furthermore, this drastic increase implies that etching of Si does not proceed from the outer surface to the inner core of Si particles; instead, it proceeds along the grain boundaries of Si particles. If etching had proceeded from the outer surface to the inner core, SSA increase would have been relatively small. In contrast, when etching proceeds along the grain boundaries of Si particles, SSA can increase immensely without producing large volume of voids. This reasoning is consistent with the TEM images shown in Fig. 5(c) and (d) where significant nano-channels rather than large voids are visible.

Fig. 6 exhibits the voltage profiles of Si/Gr@void@C etched at room temperature for 20 min. The voltage profiles during charge and discharge are in good accordance with other researchers [6,39–41], i.e., a sloping voltage profile from ~0.25 V to 0.005 V during discharge and a voltage plateau at ~0.45 V during charge. However, the capacity retention over cycles is not good. For example, the discharge specific capacity at the second cycle is 2680 mA h g $^{-1}$ , but drops to 1000 mA h g $^{-1}$  after only 10 cycles. The poor capacity retention of Si/Gr@void@C etched at room temperature for 20 min is attributed to the very limited void space in its structure (Fig. 5(a)).

Fig. 7 displays the cycling stability and CV curves of Si/ Gr@void@C composites etched with NaOH solution at 70 °C for 20 min. The cycle stability of Si/Gr@void@C composites etched at 70 °C (Fig. 7(a)) is better than that of Si/Gr@void@C composites etched at room temperature at the same current density (100 mA g<sup>-1</sup>). Specifically, the discharge capacity of Si/Gr@void@C composites etched at 70 °C is 720 mA h g<sup>-1</sup> after 20 cycles, while the corresponding value of Si/Gr@void@C composites etched at room temperature is only 500 mA h  $g^{-1}$ . Furthermore, Si/ Gr@void@C composites etched at 70 °C can be cycled up to 300 cycles with the final specific capacity at 300 mA h  $g^{-1}$ . The improved capacity retention is attributed to more voids of larger sizes in Si/Gr@void@C composites etched at 70 °C than those in Si/ Gr@void@C composites etched at room temperature. The coulombic efficiency of Si/Gr@void@C etched with NaOH solution at 70 °C for 20 min is near 100% after the first 20 cycles, indicating the presence of some irreversible processes in the first 20 cycles and minimum irreversible processes after 20 cycles.

In addition to the improved cycle stability, Si/Gr@void@C composites etched at 70 °C also exhibit good rate capability. As shown in Fig. 7(a), Si/Gr@void@C composites etched at 70 °C can still display a capacity of 300 mA h g $^{-1}$  when the current density is at 4000 mA g $^{-1}$ . After 120 cycles the rate is switched back from 2000 mA g $^{-1}$  to 1000 mA g $^{-1}$  and the capacity is recovered to 370 mA h g $^{-1}$  which is similar to the capacity at the 60<sup>th</sup> cycle with the current density at 1000 mA g $^{-1}$ . When the charge/discharge rate is switched further back to 500 mA g $^{-1}$  at the 140<sup>th</sup> cycle, the capacity increases again. At the 160<sup>th</sup> cycle the rate is further reduced to 100 mA g $^{-1}$  and the capacity further increases to 600 mA h g $^{-1}$ . All of these illustrate the possibility of fast kinetic reactions and robust stability of Si/Gr@void@C composites etched at 70 °C.

To further understand the electrochemical reactions of Si/Gr@void@C composites etched at 70 °C, cyclic voltammetry has been performed. In the CV experiments (Fig. 7(b)) the first operation is the cathodic scan starting from the open circuit voltage (~3 V vs. Li/Li<sup>+</sup>) and ending at 0.005 V. The subsequent scans are between 0.005 and 1.5 V. The peak at ~1.2 V in the first cathodic scan is due to the SEI layer formation, while the broad peak between 0.05 and 0.2 V is related to alloying of Li and Si (Li<sub>x</sub>Si) [30,42]. The 1.2 V peak disappear in the subsequent scans, indicating that most of SEI layer

formation takes place in the first scan. The broad peak in the first scan at ~2.2 V may be related to the electrochemical reactions of Li ions with trace amount of SiO<sub>2</sub> in the sample [42]. Two anodic peaks centered at 0.35 and 0.56 V are associated with the delithiation of Li-Si alloy, confirming the reversibility of the reactions in charge/discharge process [30,42]. Both of these peaks become stronger with increasing the number of scans, consistent with other studies [30,42].

To better understand the advantages of Si/Gr@void@C nanocomposites, the electrochemical performance of Si/Gr@void@C etched at 70 °C for 20 min has been compared with those of Si nanoparticles and micron-size Si particles. As shown in Fig. S4, Si/ Gr@void@C etched at 70 °C for 20 min exhibits better capacity retention than both silicon nanoparticles and micron-size silicon particles. The better performance of Si/Gr@void@C is attributed to the presence of many small voids inside the carbon shell (see Fig. 5(c) and d). These small voids act as cushion to partially accommodate the huge volume expansion of Si during lithiation, thereby minimizing volume change during cycles and offering a stable particle/electrolyte interface for SEI layer formation around the particles, postponing particle pulverization and avoiding loss of electrical contact with the conductive additive. In contrast, micronsize Si particles will experience repeated volume expansion and shrinkage, leading to fracture and re-formation of the SEI layer around the particles and thus continuous consumption of the electrolyte, increased impedance, and capacity fading [39,43]. Si nanoparticles can minimize volume change per particle and thus display better performance than micron-size Si particles, but still experience repeated volume expansion and shrinkage, thereby shorter cycle life than the Si/Gr@void@C nanocomposite (Fig. S4).

Before closing, it is worth comparing the electrochemical performance of Si/Gr@void@C nanocomposite etched at 70 °C with those reported in the literature. To do this, Fig. 7(a) has been replotted in Fig. 8. In Fig. 7(a) the specific capacity is calculated based on the active material (Si/Gr@void@C) in the electrode, whereas the specific capacity in Fig. 8 is computed based on the quantity of Si in the electrode. Based on the TGA data and TEM microstructure examination, the active material (Si/Gr@void@C) is estimated to contain 17 wt % carbon and 83 wt % Si (see Supplementary Material for details). The specific capacity in Fig. 8 can be compared with the literature directly because the specific capacity in most references is calculated based on the weight of Si only. A recent review article [1] has revealed that among 100 plus studies on Si anodes only 6 studies [8,10,12,44-46] have demonstrated Si electrodes with charge/discharge at 300 cycles or more. All of these 6 studies [8,10,12,44-46] have synthesized Si electrodes with engineered voids to accommodate huge Si expansion and shrinkage during lithiation and delithiation, respectively. These well engineered Si electrodes have exhibited remarkable battery performance. For example, a pomegranate-inspired nanoscale design for the silicon anode has exhibited battery performance with a specific capacity of 2350 and 1160 mA h  $g^{-1}$  at C/20 and C/2rates, respectively, after 1000 cycles [45]. In this pomegranate microbead structure, the Si particle structure is engineered at twolength scales. First, individual Si@C yolk-shell particles with engineered voids are formed with sizes ~100 nm. Second, these yolkshell nanoparticles are clustered together to form secondary particles of sizes 1–10 μm. This two-level length scale design offers two advantages simultaneously: (i) the electrolyte is blocked out of the cluster instead of forming SEI layers on each individual nanoparticles, and (ii) the void space in individual yolk-shell particles can accommodate the large volume change of silicon during the charge/discharge process. In spite of its outstanding performance, the synthesis procedure for making such a pomegranate-inspired Si structure is very complex and elaborated [42]. Specifically, it is synthesized through a series of processing steps including (i) coating commercial silicon nanoparticles with a SiO<sub>2</sub> layer using sol-gel process with TEOS as the precursor, (ii) self-assembling of Si@SiO2 nanoparticles in a water-in-oil emulsion to form the assembled Si@SiO2 clusters of 1-10 µm in diameter, iii) heat treatment at 550 °C for 1 h in air to remove the organics and condense the cluster structures, iv) formation of a resorcinolformaldehyde resin (RF) layer to wrap the Si@SiO<sub>2</sub> cluster, which is converted into a carbon layer under argon at 800 °C, and v) finally, the SiO<sub>2</sub> sacrificial layer is removed with 5 wt % HF solution to form the yolk-shell structure in each individual nanoparticles. In sharp contrast, the processing method established in this study is much simpler with the potential for scale-up for industrial applications. Furthermore, the present method starts with cheap micrometer Si powder to produce large quantity of nanostructured Si particles through high-energy ball milling — an industry-used method to fabricate several commercial oxide-dispersionstrengthened Ni, Fe and Al-base alloys [47–49]. Moreover, etching of partial Si using NaOH aqueous solution in the present method to create the engineered voids is safer than etching of SiO<sub>2</sub> using HF aqueous solution used to produce the pomegranate-inspired Si anode. Although the present method has the advantages of being scalable at industry environment and capable of producing low cost Si anodes, the electrochemical performance and cycle stability of Si/ Gr@void@C still need to improve significantly. This is expected to be achieved by synthesis optimization in the future, particular in the NaOH etching temperature and time to generate more and larger engineered voids to accommodate the huge volume expansion of Si during lithiation and thus achieve better cycle stability.

## 4. Concluding remarks

A facile and low cost method has been investigated in this study to prepare silicon/graphite nanocomposites with a carbonaceous coating layer and engineered voids. Pyrrole has been evaluated as the precursor to prepare the carbon coating, while partial etching of Si has been investigated using a NaOH aqueous solution to create engineered voids inside the Si/Gr nanocomposite. It is found that etching at room temperature is very slow, while at 70 °C etching becomes faster and generates noticeable voids in the Si/Gr nanocomposite. Furthermore, etching at 70 °C mainly proceeds along the grain boundaries of Si particles inside the Si/Gr@C nanocomposite. It is demonstrated that the cycle stability of Si/ Gr@void@C composites depends strongly on the engineered voids in their structure. As the volume of the engineered void increases, the cycle stability improves. This study shows that by combining high-energy ball milling, uniform carbon coating and etching at appropriate temperatures can lead to Si/Gr@void@C composites with nanostructured Si building blocks and engineered voids encapsulated in a carbon shell. Such tailored Si nanocomposites exhibit much better performance than Si nanoparticles. The best properties obtained from these tailored Si nanocomposites are about 1800 mA h  $\rm g^{-1}$  discharge capacity at the first cycle, about 580 mA h  $\rm g^{-1}$  after 40 cycles at the current density of 500 mA  $\rm g^{-1}$ , and 350 mA h g<sup>-1</sup> after 300 cycles at the current density of 100 mA g<sup>-1</sup>. Nevertheless, the synthesis method investigated in this study still needs further optimization, particularly in etching conditions to create larger voids to accommodate the huge volume expansion during lithiation and thus achieve better cycle stability.

#### Acknowledgements

MA and LS are grateful to the Rowe Family Endowment Fund, and QH acknowledges Tang Fellowship. Further, the financial support from the U.S. National Science Foundation (NSF) with the

award number CMMI-1660572 is greatly appreciated. The use of the Center for Nanoscale Materials (CNM) was supported by the U. S. Department of Energy, Office of Science, Office of Basic Energy Sciences, under Contract No. DE-AC02-06CH11357.

#### Appendix A. Supplementary data

Supplementary data related to this article can be found at https://doi.org/10.1016/j.electacta.2017.10.198.

#### References

- [1] M. Ashuri, Q. He, L.L. Shaw, Silicon as a potential anode material for Li-ion batteries: where size, geometry and structure matter, Nanoscale 8 (2016) 74–103.
- [2] N. Liu, W. Li, M. Pasta, Y. Cui, Nanomaterials for electrochemical energy storage, Front. Phys. 9 (2014) 323—350.
- [3] B. Liang, Y. Liu, Y. Xu, Silicon-based materials as high capacity anodes for next generation lithium ion batteries, J. Power Sources 267 (2014) 469–490.
- [4] X. Su, Q. Wu, J. Li, X. Xiao, A. Lott, W. Lu, B.W. Sheldon, J. Wu, Silicon-based nanomaterials for lithium-ion batteries: a review, Adv. Energy Mater. 4 (2014), 1300882-n/a.
- [5] L. Su, Z. Zhou, M. Ren, Core double-shell Si@SiO2@C nanocomposites as anode materials for Li-ion batteries, Chem. Commun. 46 (2010) 2590–2592.
- [6] M. Ashuri, Q. He, Y. Liu, K. Zhang, S. Emani, M.S. Sawicki, J.S. Shamie, L.L. Shaw, Hollow silicon nanospheres encapsulated with a thin carbon shell: an electrochemical study, Electrochim. Acta 215 (2016) 126–141.
- [7] C. Zhang, L. Gu, N. Kaskhedikar, G. Cui, J. Maier, Preparation of Silicon@Silicon oxide core—shell nanowires from a silica precursor toward a high energy density Li-lon battery anode, ACS Appl. Mater. Interfaces 5 (2013) 12340—12345.
- [8] N. Liu, H. Wu, M.T. McDowell, Y. Yao, C. Wang, Y. Cui, A yolk-shell design for stabilized and scalable Li-ion battery alloy anodes, Nano Lett. 12 (2012) 3315–3321.
- [9] X.-y. Zhou, J.-j. Tang, J. Yang, J. Xie, L.-l. Ma, Silicon@carbon hollow core—shell heterostructures novel anode materials for lithium ion batteries, Electrochim. Acta 87 (2013) 663—668.
- [10] Y. Yao, M.T. McDowell, I. Ryu, H. Wu, N. Liu, L. Hu, W.D. Nix, Y. Cui, Interconnected silicon hollow nanospheres for lithium-ion battery anodes with long cycle life, Nano Lett. 11 (2011) 2949–2954.
- [11] J. Song, S. Chen, M. Zhou, T. Xu, D. Lv, M.L. Gordin, T. Long, M. Melnyk, D. Wang, Micro-sized silicon-carbon composites composed of carbon-coated sub-10 nm Si primary particles as high-performance anode materials for lithium-ion batteries. J. Mater. Chem. A 2 (2014) 1257—1262.
- [12] R. Yi, F. Dai, M.L. Gordin, S. Chen, D. Wang, Micro-sized Si-C composite with interconnected nanoscale building blocks as high-performance anodes for practical application in lithium-ion batteries, Adv. Energy Mater. 3 (2013) 295–300.
- [13] T. Umeno, K. Fukuda, H. Wang, N. Dimov, T. Iwao, M. Yoshio, Novel anode material for lithium-ion batteries: carbon-coated silicon prepared by thermal vapor decomposition, Chem. Lett. 30 (2001) 1186–1187.
- [14] M. Yoshio, H. Wang, K. Fukuda, T. Umeno, N. Dimov, Z. Ogumi, Carbon-coated Si as a lithium-ion battery anode material, J. Electrochem. Soc. 149 (2002) A1598—A1603.
- [15] N. Dimov, K. Fukuda, T. Umeno, S. Kugino, M. Yoshio, Characterization of carbon-coated silicon: structural evolution and possible limitations, J. Power Sources 114 (2003) 88–95.
- [16] N. Dimov, S. Kugino, M. Yoshio, Carbon-coated silicon as anode material for lithium ion batteries: advantages and limitations, Electrochim. Acta 48 (2003) 1579–1587.
- [17] N. Dimov, S. Kugino, M. Yoshio, Mixed silicon—graphite composites as anode material for lithium ion batteries: influence of preparation conditions on the properties of the material, J. Power Sources 136 (2004) 108–114.
- [18] M. Yoshio, T. Tsumura, N. Dimov, Electrochemical behaviors of silicon based anode material, J. Power Sources 146 (2005) 10–14.
- [19] M. Yoshio, S. Kugino, N. Dimov, Electrochemical behaviors of silicon based anode material, J. Power Sources 153 (2006) 375–379.
- [20] M. Yoshio, T. Tsumura, N. Dimov, Silicon/graphite composites as an anode material for lithium ion batteries, J. Power Sources 163 (2006) 215–218.
- [21] N. Dimov, Y. Xia, M. Yoshio, Practical silicon-based composite anodes for lithium-ion batteries: fundamental and technological features, J. Power Sources 171 (2007) 886–893.
- [22] T. Mori, C.-J. Chen, T.-F. Hung, S.G. Mohamed, Y.-Q. Lin, H.-Z. Lin, J.C. Sung, S.-F. Hu, R.-S. Liu, High specific capacity retention of graphene/silicon nanosized sandwich structure fabricated by continuous electron beam evaporation as anode for lithium-ion batteries, Electrochim. Acta 165 (2015) 166–172.
- [23] C. Ma, C. Ma, J. Wang, H. Wang, J. Shi, Y. Song, Q. Guo, L. Liu, Exfoliated graphite as a flexible and conductive support for Si-based Li-ion battery anodes, Carbon 72 (2014) 38–46.
- [24] Y. Zhang, Y. Jiang, Y. Li, B. Li, Z. Li, C. Niu, Preparation of nanographite sheets supported Si nanoparticles by in situ reduction of fumed SiO 2 with

- magnesium for lithium ion battery, J. Power Sources 281 (2015) 425–431.
- [25] M. Su, Z. Wang, H. Guo, X. Li, S. Huang, W. Xiao, L. Gan, Enhancement of the cyclability of a Si/Graphite@ graphene composite as anode for lithium-ion batteries, Electrochim. Acta 116 (2014) 230–236.
- [26] R. Yi, J. Zai, F. Dai, M.L. Gordin, D. Wang, Dual conductive network-enabled graphene/Si—C composite anode with high areal capacity for lithium-ion batteries, Nano Energy 6 (2014) 211–218.
- [27] M. Zhang, X. Hou, J. Wang, M. Li, S. Hu, Z. Shao, X. Liu, Interweaved Si@C/CNTs&CNFs composites as anode materials for Li-ion batteries, J. Alloys Compd. 588 (2014) 206–211.
- [28] L. Shao, J. Shu, K. Wu, X. Lin, P. Li, M. Shui, D. Wang, N. Long, Y. Ren, Low pressure preparation of spherical Si@C@CNT@C anode material for lithiumion batteries, J. Electroanal. Chem. 727 (2014) 8–12.
- [29] F.-S. Li, Y.-S. Wu, J. Chou, N.-L. Wu, A dimensionally stable and fast-discharging graphite-silicon composite Li-ion battery anode enabled by electrostatically self-assembled multifunctional polymer-blend coating, Chem. Commun. 51 (2015) 8429–8431.
- [30] M. Li, J. Gu, X. Feng, H. He, C. Zeng, Amorphous-silicon@silicon oxide/chromium/carbon as an anode for lithium-ion batteries with excellent cyclic stability, Electrochim. Acta 164 (2015) 163—170.
- [31] D.-H. Lee, H.-W. Shim, D.-W. Kim, Facile synthesis of heterogeneous Ni-Si@C nanocomposites as high-performance anodes for Li-ion batteries, Electrochim. Acta 146 (2014) 60–67.
- [32] H.K. Han, C. Loka, Y.M. Yang, J.H. Kim, S.W. Moon, J.S. Cho, K.-S. Lee, High capacity retention Si/silicide nanocomposite anode materials fabricated by high-energy mechanical milling for lithium-ion rechargeable batteries, I. Power Sources 281 (2015) 293–300.
- [33] J.S. Kim, W. Pfleging, R. Kohler, H.J. Seifert, T.Y. Kim, D. Byun, H.-G. Jung, W. Choi, J.K. Lee, Three-dimensional silicon/carbon core—shell electrode as an anode material for lithium-ion batteries, J. Power Sources 279 (2015) 13–20.
- [34] Z. Guo, J. Wang, H. Liu, S. Dou, Study of silicon/polypyrrole composite as anode materials for Li-ion batteries, J. Power Sources 146 (2005) 448–451.
- [35] R. Ren, Z. Yang, L.L. Shaw, Synthesis of nanostructured silicon carbide through an integrated mechanical and thermal activation process, J. Am. Ceram. Soc. 85 (2002) 819–827.
- [36] Z.-G. Yang, L.L. Shaw, Synthesis of nanocrystalline SiC at ambient temperature through high energy reaction milling, Nanostructured Mater. 7 (1996)

- 873-886.
- [37] L. Chen, Y. Liu, M. Ashuri, C. Liu, L.L. Shaw, Li2S encapsulated by nitrogen-doped carbon for lithium sulfur batteries, J. Mater. Chem. A 2 (2014) 18026—18032.
- [38] J. Hong, M.K. Park, E.J. Lee, D. Lee, D.S. Hwang, S. Ryu, Origin of new broad Raman D and G Peaks in annealed graphene, Sci. Rep. 3 (2013) 2700.
- [39] L. Pan, H. Wang, D. Gao, S. Chen, L. Tan, L. Li, Facile synthesis of yolk—shell structured Si—C nanocomposites as anodes for lithium-ion batteries, Chem. Commun. 50 (2014) 5878—5880.
- [40] M. Obrovac, L. Krause, Reversible cycling of crystalline silicon powder, J. Electrochem. Soc. 154 (2007) A103—A108.
- [41] H. Kim, M. Seo, M.-H. Park, J. Cho, A critical size of silicon nano-anodes for lithium rechargeable batteries, Angew. Chem. Int. Ed. 49 (2010) 2146–2149.
- [42] Z. Sun, X. Song, P. Zhang, L. Gao, Controlled synthesis of yolk-mesoporous shell Si@SiO2 nanohybrid designed for high performance Li ion battery, RSC Adv. 4 (2014) 20814–20820.
- [43] C.K. Chan, H. Peng, G. Liu, K. McIlwrath, X.F. Zhang, R.A. Huggins, Y. Cui, High-performance lithium battery anodes using silicon nanowires, Nat. Nanotechnol. 3 (2008) 31–35.
- [44] L.Y. Yang, H.Z. Li, J. Liu, Z.Q. Sun, S.S. Tang, M. Lei, Dual yolk-shell structure of carbon and silica-coated silicon for high-performance lithium-ion batteries, Sci. Rep. 5 (2015).
- [45] N. Liu, Z. Lu, J. Zhao, M.T. McDowell, H.-W. Lee, W. Zhao, Y. Cui, A pomegranate-inspired nanoscale design for large-volume-change lithium battery anodes, Nat. Nanotechnol. 9 (2014) 187–192.
- [46] H. Wu, G. Chan, J.W. Choi, I. Ryu, Y. Yao, M.T. McDowell, S.W. Lee, A. Jackson, Y. Yang, L. Hu, Y. Cui, Stable cycling of double-walled silicon nanotube battery anodes through solid-electrolyte interphase control, Nat. Nanotechnol. 7 (2012) 310–315.
- [47] P. Gilman, J. Benjamin, Mechanical alloying, Annu. Rev. Mater. Sci. 13 (1983)
- [48] J.S. Benjamin, T.E. Volin, The mechanism of mechanical alloying, Metall. Trans. 5 (1974) 1929–1934.
- [49] F.H. Froes, J.J. DeBarbadillo, Structural applications of mechanical alloying, in: Proceedings of an ASM International Conference, Myrtle Beach, South Carolina, 27–29 March 1990, ASM International, 1990.